Region-specific regulation of stem cell-driven regeneration in tapeworms

Tania Rozario[1*], Edward B. Quinn[1], Jianbin Wang[2], Richard A. Davis[2], and Phillip A. Newmark[1,3,4*]

[1]Morgridge Institute for Research, Madison, WI, USA, [2]Department of Biochemistry and Molecular Genetics, RNA Bioscience Initiative, University of Colorado School of Medicine, Aurora, CO, USA, [3] Howard Hughes Medical Institute, [4]Department of Integrative Biology, University of Wisconsin-Madison, Madison, WI, USA.

* corresponding authors

Email: trozario@morgridge.org

pnewmark@morgridge.org

Abstract

Tapeworms grow at rates that rival all metazoan tissues, including during embryonic and neoplastic growth. For example, the rat intestinal tapeworm, *Hymenolepis diminuta*, produces up to 2,200 proglottids (segments), increasing in length up to 3,400 fold, and weight up to 1.8 million fold within the first 15 days of infection[1]. Tapeworms also regenerate: they shed large parts of their body, releasing their embryos to continue their life cycle, yet are able to continuously replenish proglottids and maintain an equilibrium length. Such remarkable growth and regeneration are fueled by adult somatic stem cells, which have yet to be characterized molecularly. Using *H. diminuta* as a laboratory model, we find that regeneration is limited to the tapeworm neck, making this tissue a prime source to identify stem cell genes. Using transcriptomic analyses and RNA interference (RNAi), we characterize and functionally validate the first molecular regulators of tapeworm growth and regeneration. However, we find no evidence that stem cells are restricted to the regeneration-competent neck. Instead, we find that lethally irradiated tapeworms can be rescued from death when cells from both regeneration-competent and regeneration-incompetent regions are transplanted into the neck. Furthermore, the persistence of regenerative ability over time requires signal(s) from the head, even though the head itself cannot regenerate and the head is not necessary for initial regeneration. Together, the head and neck tissue provide a microenvironment that regulates stem cells to enable region-specific regeneration in this tapeworm.

34 **Introduction**

35

36 Tapeworms are parasitic flatworms that infect humans and livestock, causing lost
37 economic output, disease, and in rare cases, death[2]. Tapeworms are well known for their ability to
38 reach enormous lengths. For example, humans infected with the broad or fish tapeworm,
39 *Diphyllobothrium latum*, harbor parasites that average 6 m in length[3]. It is less commonly
40 appreciated that tapeworms regenerate to accommodate their multi-host life cycle. Adult
41 tapeworms in their host intestine develop proglottids that are gravid with embryos. Tapeworms
42 pinch off the posterior and gravid sections of their body, which exit with the host excrement, to be
43 eaten by a suitable intermediate host that supports larval tapeworm development. In spite of losing
44 large body sections, the tapeworm does not progressively shorten; instead, it regenerates
45 proglottids to maintain an equilibrium length. Despite this remarkable biology, tapeworms are an
46 unexplored animal model in the study of regenerative behaviors.

47 Up until the 1980s, the rat intestinal tapeworm, *H. diminuta*, had been a favorite model
48 organism among parasitologists because these parasites are easily propagated in the laboratory. A
49 great deal of work in cell biology, biochemistry, physiology, and electron microscopy has enriched
50 our understanding of these tapeworms[4]. With the dawn of the molecular age and the preference
51 among scientists to concentrate on a handful of model organisms, *H. diminuta* was largely left
52 behind.

53 As an obligate endoparasite, adult *H. diminuta* will expire once its host rat dies. However,
54 the lifespan of *H. diminuta* can be uncoupled from that of its host. A single adult tapeworm can be
55 serially amputated and transplanted into a new host intestine, where the fragment can regenerate
56 into a mature tapeworm, even after 13 rounds of amputation over 14 years[5]. These observations

57 have led to speculation that *H. diminuta* may be inherently immortal, though their life span is
58 limited by that of their host. This longevity is reminiscent of the free-living cousins of tapeworms:
59 freshwater planarians like *Schmidtea mediterranea.* Asexual *S. mediterranea* can reproduce
60 indefinitely by fission, and can regenerate its whole body from tiny fragments. Planarian
61 immortality and regeneration are enabled by adult somatic stem cells called neoblasts[6-8]. These
62 stem cells are the only dividing cells within the soma. Like planarians, *H. diminuta* maintains a
63 population of neoblast-like adult somatic stem cells[9] that are likely responsible for their growth
64 and regenerative ability. Recently, stem cells of other parasitic flatworms have been defined
65 molecularly, and their maintenance depends on conserved factors such as argonaute family
66 members and fibroblast growth factor signaling[10-12]. However, key differences also exist, as a
67 number of conserved stem cell genes, like *piwi, vasa,* and *tudor,* are absent from the genomes of
68 parasitic flatworms[13].

69 Mechanisms of stem cell regulation in parasitic flatworms are still largely unexplored,
70 though stem cells are crucial for parasite biology and even disease. For example, the tapeworm
71 *Echinococcus multilocularis* causes alveolar echinococcosis, in which larvae use their stem cells
72 to grow as infiltrative cysts that can cause organ failure, and like a malignant tumor, can
73 metastasize to secondary organs[14]. A better understanding of stem cell regulation in parasitic
74 flatworms is needed to elucidate parasite biology and potentially, for gaining therapeutic insights.

75 In this study, we use *H. diminuta* to investigate the molecular basis of tapeworm
76 regeneration. We established and refined experimental tools such as transcriptomics, *in vitro*
77 parasite culture, RNA *in situ* hybridization, cycling cell tracing with thymidine analogs, and RNA
78 interference (RNAi), all reported in this work. We determine that the ability to regenerate is
79 regionally limited to the neck of adult *H. diminuta*. However, regeneration from the neck is finite

80 without signals from the tapeworm head. Using RNA sequencing (RNA-seq), we identify and
81 characterize various markers of the somatic cycling cell population, which includes tapeworm stem
82 cells. We functionally validate essential regulators of growth and regeneration. Intriguingly, our
83 analyses failed to uncover a neck-specific stem cell population that explains the regional
84 regenerative ability displayed by *H. diminuta.* Instead, we demonstrate that tapeworm regeneration
85 can be rescued by cells that are sourced from outside the neck, regardless of source-tissue
86 regeneration competence. Thus, extrinsic signals present in the tapeworm neck confer region-
87 specific regenerative ability in this tapeworm.

88 **Results and Discussion**

89

90 To examine the regeneration competence of *H. diminuta*, we amputated different
91 anatomical fragments cut from the adult and assayed their ability to regenerate. The body plan of
92 adult *H. diminuta* consists of a head with four suckers, an unsegmented neck (~2.5-3 mm in 6-day
93 old worms), and a body with thousands of proglottids that grow and mature in an anterior-to-
94 posterior direction (Fig. 1a). Previous work showed that amputated *H. diminuta* anterior fragments
95 transplanted into rat intestines were able to regenerate into mature tapeworms[5,15]. However, using
96 transplantation, a complete study of regeneration competence was not possible: only anterior
97 fragments could be tested because the suckers are required to anchor the worms to the intestine.
98 To ascertain which anatomical regions of *H. diminuta* are competent to regenerate, amputated
99 fragments must be grown *in vitro*. We successfully established *H. diminuta in vitro* culture
100 modified from the Schiller method[16], and tested the regeneration competence of several different
101 1 cm fragments (Fig. 1b-c). The anterior-most fragments (head + neck + body) were competent to
102 regenerate, confirming previous observations using amputation and transplantation[5,15].
103 Additionally, anterior fragments that were first decapitated (neck + body) were also competent to
104 regenerate proglottids. In contrast, "body only" fragments that did not contain the neck tissue were
105 not competent to regenerate proglottids. All amputated fragments could grow in length (Fig. 1d),
106 differentiate mature reproductive structures, and mate. However, the neck is necessary for
107 regeneration of new proglottids over time. In no case did we observe head regeneration. Also,
108 amputated heads alone could not regenerate proglottids *in vitro* (data not shown) nor *in vivo*[15]. To
109 test if the neck is sufficient for proglottid regeneration, we amputated 2 mm fragments of the neck
110 tissue and grew the fragments *in vitro*. "Neck only" fragments regenerated an average of 383

111 proglottids (SD=138, n=20) after 12 days *in vitro* (Fig. 1e). Thus, the tapeworm neck is both
112 necessary and sufficient for proglottid regeneration.

113 Previous studies have shown that *H. diminuta* can regenerate after serial rounds of
114 amputation and transplantation for over a decade[5] and perhaps indefinitely. Using *in vitro* culture,
115 we confirmed that anterior fragments of *H. diminuta* can regenerate proglottids after four rounds
116 of serial amputation followed by 12-15 days of *in vitro* culture (Fig. 1f-g) without any observable
117 cessation of regenerative ability. Decapitated fragments were competent to regenerate proglottids
118 after the first amputation; however, re-amputation abrogated regeneration (Fig. 1f-g). After
119 decapitation, a definitive neck tissue could not be maintained and eventually, the whole tissue was
120 comprised of proglottids (Fig. S1). Without the head, proglottid regeneration from the neck is
121 finite. Thus, the tapeworm head is necessary for persistent proglottid regeneration and to maintain
122 an unsegmented neck.

123 If signals from the head regulate regeneration, is regenerative potential asymmetric across
124 the anterior-posterior (A-P) axis of the neck? We subdivided the neck into three 1 mm fragments
125 and assayed the number of proglottids regenerated *in vitro* (Fig. 1h-i). We found that the most
126 anterior neck fragments regenerated more proglottids than the middle or posterior neck fragments
127 (Fig. 1h-i). Thus, only the neck is competent to regenerate proglottids, but signals from the head
128 also regulate regeneration, resulting in an anterior bias in regenerative potential.

129 Why is the neck the only region competent to regenerate? One hypothesis is that pluripotent
130 stem cells are confined to the neck. There are currently no specific molecular markers for adult
131 tapeworm stem cells. However, like in other flatworms, the only proliferative somatic cells in *H.*
132 *diminuta* are undifferentiated[17,18]. Thus, cycling somatic cells include tapeworm stem cells and
133 any dividing progeny. To label cycling somatic cells, we used two methods: uptake of the

134 thymidine analog F-ara-EdU to mark cells in S-phase and fluorescent RNA *in situ* hybridization
135 (FISH) against conserved cell cycle-regulated transcripts such as the replication licensing factor
136 *minichromosome maintenance complex component 2* (*mcm2*) and *histone h2b* (*h2b*). Both *h2b* and
137 *mcm2* are conserved cycling cell markers expressed in stem cells of free-living and parasitic
138 flatworms[10,19]. We detected cycling somatic cells throughout the tapeworm body (Fig. S2a-c).
139 Contrary to previous results[17], we also detected cycling cells in the head, though in small numbers.
140 The scarcity of these cycling cells may be the reason they were originally missed. Taken together,
141 cycling cells are present in tissues that are competent or incompetent to regenerate proglottids.
142 Though cycling cells are widely distributed, it is possible that within this population, there
143 are stem cells of varying potency and that a pluripotent subpopulation may be restricted to the
144 neck. To identify potential stem cell markers, we characterized the cycling cell population at the
145 molecular level. Previously, stem cell genes had been identified in flatworms using irradiation to
146 deplete cycling cells followed by transcriptome analysis to identify downregulated
147 transcripts[10,19,20]. In *H. diminuta*, cycling cells are undetectable after exposure to 200 Gy irradiation
148 (Fig. S2d). Consequently, growth and regeneration were also stunted following irradiation (Fig.
149 2a-b). We leveraged the sensitivity of *H. diminuta* to irradiation to identify new molecular markers
150 of cycling somatic cells, including stem cells. Untreated and irradiated worms were cultured *in*
151 *vitro* for 3 days, after which the necks were amputated and processed for RNA-seq (Fig. 2c). We
152 assembled a *de novo* transcriptome for *H. diminuta* consisting of 14,346 transcripts (refer to
153 methods) to which sequencing reads were mapped. Using differential gene expression analysis,
154 we identified 683 irradiation-sensitive transcripts (downregulated; FDR ≤0.05) (Supplemental
155 Table 1), cloned 335 genes, and examined their expression patterns using whole-mount
156 colorimetric *in situ* hybridization (WISH). Using WISH, we observed that expression of

157 irradiation-sensitive genes was indeed reduced after exposure to irradiation, validating our RNA-
158 seq approach (Fig. S3).

159 In tapeworms, the position of cycling cells in the neck is spatially restricted in a pattern
160 that is conserved in multiple tapeworm species[21] (Fig. 2d-e). Cycling cells are located in the neck
161 parenchyma, which is bounded by the nerve cords. Cycling cells are not found at the animal edge
162 where differentiated cells of the muscle and tegument (parasite skin) are located[17]. This pattern
163 allowed us to use WISH to identify potential cycling cell genes. After excluding genes with
164 ubiquitous expression or poor signal by WISH, we examined gene expression for 194 irradiation-
165 sensitive genes. 62% of genes examined were expressed in the neck parenchyma, though in a
166 variety of patterns (Fig. S4a). 13% of genes examined were predominantly expressed in the neck
167 parenchyma, similar to *h2b* and *mcm2* (Fig. 2f, S4b). These include the nucleic acid binding factor
168 *Zn finger MYM type 3* (*zmym3)*, the transcription factor *suppressor of hairy wing* (*su(Hw)*), nuclear
169 lamina component *laminB receptor* (*lbr*), and *leucine-rich WD-containing gene* (*lrwd*). 25% of
170 irradiation-sensitive genes, were expressed in a minority of cells in the neck parenchyma (Fig.
171 S4c). 24% were expressed broadly, including within the neck parenchyma and at the animal edge
172 where non-cycling differentiated cells are located (Fig. S4d). In conclusion, irradiation-sensitive
173 genes identified by RNA-seq likely represent markers for stem cells, progenitors, and even
174 differentiated cells that were lost or compromised following irradiation.

175 To ascertain whether genes that showed expression in the neck parenchyma were indeed
176 expressed in cycling cells, we performed double fluorescent *in situ* hybridization (dFISH) with
177 candidate genes and either *h2b* or *mcm2.* We use *h2b* and *mcm2* interchangeably as they
178 completely co-localize in the neck parenchyma (Fig. S5). Irradiation-sensitive genes from Fig. 2f
179 were indeed expressed in cycling somatic cells (Fig. 2g-h, S6a-b). One gene, the homeobox factor,

180 *prospero* (*pros*), was expressed exclusively in a subset of cycling cells (Fig. 2i). We confirmed
181 that irradiation-sensitive genes that only partially overlapped in the neck parenchyma, such as the
182 Zn finger-containing genes *HDt_10981* and *HDt_05316* were expressed in a subset of cycling cells
183 as well as non-cycling differentiated cells (Fig. S6c-d). We propose that these genes represent
184 lineage-committed stem cells or progenitors for tissues such as muscle, neurons, tegument, or
185 protonephridia. In summary, we performed dFISH for 53 candidates and found that 72% of genes
186 tested were co-expressed in cycling cells (Fig. S6e, Supplemental Table 2). Our analysis revealed
187 that there is a heterogeneous and complex mixture of cell types or states within the cycling cell
188 population.

189 We reasoned that genes expressed in the majority of cycling cells would likely be essential
190 for tapeworm growth and may regulate stem cell populations that are necessary for regeneration.
191 Thus, we developed an RNAi protocol that allowed us to functionally investigate how candidate
192 genes affect tapeworm growth and regeneration (Fig. 3a). As a proof of principle, we used RNAi
193 to knock down *h2b.* Stem cells are constantly dividing and require new histone synthesis to
194 maintain the population. Thus, downregulating expression of *h2b* in tapeworms would likely
195 compromise growth as a result of cycling cell loss, as is the case in other flatworms[19,22]. In our
196 RNAi paradigm, knockdown of *h2b* induced gross growth defects (Fig. 3b-c). The number of
197 proglottids regenerated was also reduced; however, this was difficult to quantify as many RNAi
198 worms were so thin and frail that proglottid definition was lost. We then tested two newly
199 identified cycling cell genes: *zmym3,* and *su(Hw)* for potential roles in tapeworm growth and
200 regeneration. Similar to knockdown of *h2b, zmym3(RNAi)* and *su(Hw)(RNAi)* each resulted in
201 abrogated growth and regeneration. RNAi-mediated knockdown has been demonstrated in other
202 tapeworm species[23-26], though not in *H. diminuta.* RNAi has not been widely adopted for studying

203 tapeworm biology due to technical challenges, like poor knockdown efficacy, inefficient
204 penetrance, and the difficulty of *in vitro* culture. Our RNAi scheme is relatively straightforward
205 and robust, and shows that gene inhibition can be used to uncover regulators of adult tapeworm
206 growth and regeneration.

207 Are the growth defects we observe the consequence of defects in the cycling cell
208 population? After RNAi, we quantified the number of cycling cells present by detecting F-ara-
209 EdU^+ cells following 1-hour exposure to the thymidine analog. Knockdown of *h2b, zmym3,* and
210 *su(Hw)* severely reduced the number of cycling cells detectable in the neck (Fig. 3d-e). Thus, *h2b,*
211 *zmym3,* and *su(Hw)* are necessary for the function of cycling cells.

212 The mechanism of action by *zmym3* and *su(Hw)* in *H. diminuta* is currently unknown. In
213 mice and humans, *zmym3* acts as a transcriptional repressor with chromatin-binding properties and
214 has been shown to regulate cell cycle progression[27] and DNA repair[28]. In *Drosophila*, *su(Hw)* binds
215 to *gypsy* insulator sequences to regulate chromatin silencing[29]. Similar functions for these genes
216 may be conserved in tapeworms as cell cycle regulation, DNA repair, and silencing are likely
217 important for the regulation of tapeworm stem cells.

218 We have now described molecular heterogeneity within the cycling cells of the neck
219 parenchyma and identified *h2b, zmym3,* and *su(Hw)* as functionally important in cycling cell
220 regulation. At this point, we have not yet determined why regeneration competence is restricted to
221 the neck. Are subsets of cycling cells distributed in a polarized manner? No gene expression pattern
222 examined was exclusive to cycling cells of the neck. By WISH, all cycling cell genes were
223 expressed throughout the whole tapeworm body, including *zmym3* and *su(Hw)* (Fig. 4a). Since we
224 observed an anterior bias in regenerative ability (Fig. 1h-i), we hypothesized that stem cells may
225 be asymmetrically distributed in the neck and detectable by RNA-seq. We performed RNA-seq of

226 1 mm anterior, middle, and posterior neck fragments (Fig. 1h) and identified 454 anterior-enriched
227 and 238 anterior-depleted transcripts (Fold change ≥1.5 or ≤-1.5 respectively; FDR ≤0.05) and
228 overlaid them with our irradiation-sensitive dataset. The majority of anterior-enriched transcripts
229 (88%) were not irradiation sensitive (Fig. S7a). Instead, we observed that anterior-enriched and
230 anterior-depleted genes were often expressed in corresponding gradients (Fig. 4b) but these
231 patterns were not within the neck parenchyma. Our results suggest that the polarized signals across
232 the neck tissue are predominantly within the non-cycling compartments.

233 Since our RNA-seq analysis identified transcripts that were anterior-enriched and
234 irradiation-sensitive (Fig. S7a), we examined their expression patterns to ascertain if these genes
235 are expressed within stem cells. We found 15 genes that are expressed in a subset of cells within
236 the neck parenchyma, including *pros*, *solute carrier family 13* (*slc13*), *hepatocyte nuclear factor*
237 *4* (*hnf4*), and several novel genes (Fig. S7b). However, by dFISH with *mcm2*, 7/8 genes tested
238 were not expressed in cycling cells (Fig. S7c). Only one gene, *pros,* was co-expressed in cycling
239 cells (Fig. 2i). Our analyses have not revealed an anteriorly biased subpopulation of stem cells that
240 confer regenerative ability. This may be due to the coarse resolution of our analysis. A more
241 thorough characterization of tapeworm cycling cells by single-cell RNA-seq is warranted.
242 Nonetheless, the variety of cycling cell markers we have described in this work will aid in future
243 classification of tapeworm stem cells.

244 So far, we have not found evidence for a unique neck-specific subpopulation of cycling
245 cells. This led us to hypothesize that stem cells may be distributed throughout the tapeworm, but
246 that extrinsic signals operating in the neck are necessary to instruct stem cell behavior and/or
247 proglottid regeneration. To pursue this hypothesis, we designed a functional assay to test
248 populations of cells for the ability to rescue regeneration. We exposed tapeworms to a lethal dose

249 of irradiation, injected wild-type cells into the neck region, amputated 5 mm anterior fragments,
250 and looked for rescue of viability and regeneration after 30 days *in vitro*. Remarkably, bulk-cell
251 transplants were able to rescue irradiated worms that were destined to die (Fig. 4c; 44% rescue
252 (n=41)). In no case did we observe rescue of viability or regeneration in irradiated worms that were
253 not injected with cells or mock-injected (n=34). With this functional assay in hand, we compared
254 cells from tapeworm anteriors (including the regeneration-competent neck) to cells from tapeworm
255 posteriors (which are regeneration incompetent) for rescue ability. We found that cells from both
256 regeneration-competent and regeneration-incompetent regions of *H. diminuta* were able to recue
257 viability and regeneration in lethally irradiated tapeworms (Fig. 4d; 11% rescue for both A and P
258 (n=37 and 35, respectively)). These results confirm that the regeneration competence of the neck
259 tissue is not due exclusively to intrinsic properties of stem cells in this region, but to extrinsic
260 signals that regulate competence to regenerate.

261 Our results suggest that in tapeworms, location matters enormously: the head and neck
262 environment provide cues that regulate the ability of stem cells to mediate proglottid regeneration.
263 We show that the head plays instructive roles that regulate how proglottids form and regenerate.
264 Signals from the head may create gradients across the neck that inhibit proglottidization and are
265 necessary to maintain the neck as an unsegmented tissue. Proglottids can only form once the
266 inhibitory signals are sufficiently diminished (Fig. 4e). How the head regulates stem cells is less
267 clear. The head may serve as a niche (directly or indirectly) that is necessary for the maintenance
268 of stem cells in the neck (Fig. 4e). In this model, stem cells are collectively pluripotent only when
269 they receive head-derived niche signals, thus limiting regenerative potential to the neck.
270 Alternatively, stem cells may depend on a local niche that is independent of the head (Fig. 4e). In
271 this model, stem cells have the capacity to form all cell lineages from any amputated fragment,

272 however, the extrinsic signals that activate proglottid formation are only found in the neck. The
273 interplay between intrinsic and extrinsic stem cell regulatory signals has already been shown to
274 play important roles in regeneration. Head regeneration was induced in three planarian species that
275 were naturally regeneration deficient by manipulating the gradient of wnt signaling by RNAi[30-32].
276 These planarians maintained pluripotent stem cells but could not regenerate heads because of
277 inhibitory cues from the surrounding tissue. In tapeworms, gradients of wnt signaling that delineate
278 A-P polarity are conserved with planarians[33]. RNA-sequencing of the neck A-P axis in *H. diminuta*
279 has revealed genes that are expressed in gradients across the neck, which could help us understand
280 how stem cells and regeneration depend on these extrinsic signals.

281 **Materials and Methods**

282

283 Animal care and use

284 Infective *H. diminuta* cysts were obtained from Carolina Biologicals (132232). To obtain
285 adult tapeworms, 100-300 cysts were fed to Sprague-Dawley rats by oral gavage in ~0.5 mL of
286 0.85% NaCl. Rats were euthanized in a CO_2 chamber typically 6 days post-gavage and tapeworms
287 were flushed out of the small intestine and washed in 1X Hanks Balanced Salt Solution (HBSS;
288 Corning) (140 mg/L $CaCl_2$, 100 mg/L $MgCl_2.6H_2O$, 100 mg/L $MgSO_4.7H_2O$, 400 mg/L KCl, 60
289 mg/L KH_2PO_4, 350 mg/L $NaHCO_3$, 8 g/L NaCl, 48 mg/L Na_2HPO_4, 1 g/L D-glucose, no phenol
290 red). Rodent care was in accordance with IACUC policies and protocols.

291

292 *In vitro* parasite culture

293 Biphasic parasite cultures were prepared based on the Schiller method[16]. Briefly, the solid
294 phase was made in 50 mL Erlenmeyer flasks by mixing 30% heat-inactivated defibrinated sheep
295 blood (Hemostat) with 70% agar base for 10 mL blood-agar mixture per flask. Fresh blood was
296 heat-inactivated at 56°C for 30 min then kept at 4°C and used repeatedly for one week by first
297 warming the blood to 37°C. The agar base was prepared from 8 g Difco nutrient agar and 1.75 g
298 NaCl in 350 mL water, autoclaved, and stored at 4°C. Before use, the agar base was microwaved
299 to liquify, and cooled to below 56°C before mixing with warmed blood. After the blood-agar
300 mixture solidified, 10 mL of Working Hanks 4 (WH4; 1X HBSS/4 g/L total glucose/1X antibiotic-
301 antimycotic (Sigma)) was added. Each flask was topped with a gas-permeable stopper (Jaece
302 Identi-plug) and pre-incubated at 37°C in hypoxia (3% CO_2/5% O_2/95% N_2) overnight before use.
303 Before tapeworms were transferred into the flasks, the liquid phase was adjusted to pH7.5 with

304 200 μL 7.5% $NaHCO_3$ (Corning). Tapeworms were first washed in WH4 for 10 mins at 37°C in
305 petri dishes pre-coated with 0.5% BSA to inhibit sticking. Transfers to pre-cultured flasks were
306 performed by gently lifting the worms with a stainless-steel hook (Moody Tools) and immersing
307 them in the liquid phase. Tapeworms were transferred to fresh cultures every 3 days.
308
309 Fixation and Staining
310 Tapeworms were heat-killed by swirling in 75-80°C water for a few seconds until the
311 worms relaxed and elongated, then fixative (4% formaldehyde/10% DMSO/1% NP40 in
312 Phosphate Buffered Saline with 0.3% TritonX-100 (PBSTx)) was added immediately. Tapeworms
313 were fixed for 30 min-2hr at room temperature or overnight at 4°C. For DAPI staining, samples
314 were incubated in 1 μg/mL DAPI (Sigma) in PBSTx overnight at 4°C. Stained tapeworms were
315 cleared in 80% glycerol/10 mM Tris pH7.5/1 mM EDTA overnight at room temperature before
316 mounting.
317
318 Thymidine analog uptake and staining
319 For BrdU pulse, tapeworms were incubated in 10 μM BrdU (Sigma) in 1% DMSO at 37°C
320 in WH4 and processed for staining by an adapted protocol previously used on planarians[34] and
321 schistosomes[10]. Tapeworms were killed in cold 2% HCl for 2 min with shaking every 30 seconds,
322 fixed in cold methacarn (6:3:1 methanol:chloroform:glacial acetic acid) for 30 min at 4°C.
323 Denaturation was performed in 2N HCl for 45 min. Blocking and antibody incubation were
324 performed in K-block (5% Horse serum/0.45% fish gelatin/0.3% Triton-X/0.05% Tween-20/PBS)
325 [35], before detection with anti-BrdU antibody (1:500, B35128, Invitrogen) and anti-mouse-HRP

326 secondary antibody (1:1000; Jackson). Tyramide signal amplification (TSA) reaction[36] was also
327 used.

328 For F-ara-EdU pulse, tapeworms were incubated in 0.1 μM F-ara-EdU (Sigma) in 1%
329 DMSO for 1 hr at 37°C in WH4. Tapeworms were heat-killed, fixed in 4% formaldehyde/10%
330 DMSO/1% NP40/PBSTx, permeabilized by treatment with 10 μg/mL Proteinase-K/0.1%
331 SDS/PBSTx for 10-30 min at room temperature, fixed in 4% formaldehyde/PBSTx for 10 min
332 before samples were cut into small pieces or retained whole in PBSTx. Samples were
333 permeabilized in PBSTx/10% DMSO/1% NP40 for 20min-1 hr (depending on size) before
334 performing the click-it reaction[37] with Oregon Green 488 Tyramide (Invitrogen). Signal was
335 detected using anti-Oregon Green 488-HRP antibody (1:1000; A-21253 Invitrogen) in K-block
336 followed by TSA reaction. For F-ara-EdU quantification, tiled confocal z-stacks through the
337 anterior of the worms were taken and cell numbers were counted using background subtraction on
338 Imaris.

339

340 Irradiation

341 Irradiation was performed using a CellRad irradiator (Faxitron Bioptics) at 200 Gy (150
342 kV, 5 mA). Tapeworms were irradiated in WH4 in BSA-coated petri dishes. At this dosage,
343 tapeworms degenerated and were inviable after 30 days in culture.

344

345 Transcriptome assembly

346 To construct a transcriptome for *H. diminuta,* we collected RNA from five regions: 1) head
347 and neck, 2) immature proglottids, 3) mature reproductive proglottids, 4) gravid proglottids, and
348 5) mixed larval stages isolated from beetles. The first three regions covered the entirety of 3.5-

349 week old adult tapeworms. The gravid proglottids were taken from the posteriors of 10-week old
350 tapeworms. Paired-end libraries were constructed with 2 x 150 bp reads from a HiSeq2500 chip.
351 2 x ~30 million reads were obtained for each sample. The transcriptome was assembled from three
352 components: 1) map-based assembly, 2) *de novo* assembly, and 3) Maker predictions from
353 Wormbase Parasite. The map-based assembly was performed using TopHat2 with the 2014 *H.*
354 *diminuta* draft genome courtesy of Matt Berriman at the Wellcome Sanger Institute. 15,859
355 transcripts were assembled using TopHat. *De novo* assembly was performed using Velvet/Oases
356 and resulted in 144,682 transcripts. For the Maker predictions, there were 11,275 predicted
357 transcripts and 73.2% matched (>95% along the length) to the TopHat transcripts. The remaining
358 predicted transcripts that were not represented in the TopHat dataset were added to make a
359 combined TopHat/predicted set of 17,651 transcripts. Most of the Oases transcripts matched to the
360 TopHat/predicted set but 35,300 or 24.4% of the Oases transcripts did not (>75% match cut-off).
361 These transcripts could be transcripts missed in the genome, transcription noise, non-coding
362 transcripts, or contamination. We found significant contamination from beetle tissue in the larval
363 tapeworm sample (more below). Initial filtering for contamination excluded 1,388 transcripts
364 (from beetle, rat, bacterial, and viral sources). At this point 51,563 transcripts were retained from
365 the three methodologies described above and were processed for further filtering.

366 We first filtered out additional contamination from beetle tissues. We expect that this was
367 a large problem because during dissections, beetle tissues adhered to the tapeworm larvae and were
368 not easily washed away. These transcripts had best hits to beetle proteins (from *Ixodes scapularis,*
369 *Harpegnathos saltator, Monodelphis domestica, Nasonia vitripennis, Pediculus humanus*
370 *corporis, Solenopsis invicta, Tenebrio molitor,* and *Tribolium castaneum*). Most of the transcripts
371 were from the Oases *de novo* assembly and did not match the *H. diminuta* genome. Furthermore,

372 they were strongly over-represented in the larval sample only. Thus, an additional contamination
373 filtering step was taken: transcripts from the Oases assembly without matches to the *H. diminuta*
374 genome that showed >90% expression (by RPKM) in the larval sample were filtered out as
375 potential contaminants. 11,918 transcripts were filtered out in this step.

376 To the remaining 39,645 transcripts, we applied additional filters: 1) Remove transcripts if
377 average RPKM<1 unless the transcript is long (>1000 bp), has a long ORF (>500 bp) or is
378 annotated. 11,615 transcripts were removed as they met none of these criteria. 2) A stringent
379 expression cut-off was applied to the remaining Oases transcripts; transcripts were discarded if
380 average RPKM<5 and maximum RPKM<10 unless the transcripts were long (>1000 bp), had long
381 ORFs (>500 bp) or were annotated. 8,027 transcripts were removed. 3) 51 transcripts were
382 removed because they are mitochondrial or rRNAs. 4) An ORF size filter was applied to remove
383 all transcripts with ORF <300 bp unless they are annotated. 5,331 transcripts were removed. 5)
384 For the Maker predicted transcripts, expression and size filters were applied to remove transcripts
385 with expression <1 RPKM and size <500 bp. 275 transcripts were removed.

386 Our final transcriptome is comprised of 14,346 transcripts (84.9% TopHat, 8.4% Maker
387 predictions, 6.1% Oases with match to genome, and 0.6% Oases without match to genome). The
388 total transcriptome size is 34 Mb with average transcript length of 2,354 bp.

389

390 <u>RNA-seq for differential gene expression analyses</u>

391 Tissue was collected and immediately frozen on dry ice in 100 μL Trizol (Life
392 Technologies) before RNA extraction. Tissue homogenization was performed as the mixture was
393 in a semi-frozen state using RNase-free pestles and a pestle motor. RNA was purified using the
394 Direct-zol RNA MiniPrep kit (Zymo). RNA quality was assessed using Bioanalyzer, libraries were

395 prepared with TruSeq Stranded mRNAseq Sample Prep kit (Illumina), and sequenced on two lanes
396 on a HiSeq2500 chip. We performed paired-end sequencing and obtained ~20 million reads per
397 sample. Samples were obtained in triplicate. To identify irradiation-sensitive genes, 2 mm anterior
398 tapeworm fragments were cut from 10 worms after 3 days *in vitro*. To identify differentially
399 expressed transcripts across the neck A-P axis, 1 mm fragments were cut from 20 freshly obtained
400 6-day old tapeworms. Differential gene expression analysis was performed using CLC Genomics
401 Workbench (Qiagen) by mapping to our assembled transcriptome (above).
402
403 *In situ* hybridization
404 WISH and FISH protocols were modified from previously published methods for
405 planarians[36] and the mouse bile-duct tapeworm *Hymenolepis microstoma* (Peter Olson, personal
406 communication). Tapeworms were heat killed and fixed in 4% formaldehyde/10% DMSO/1%
407 NP40/PBSTx for 30 min at room temperature before washing and dehydration into methanol.
408 Dehydrated samples were kept at -30°C for at least 2 days. After rehydration, samples were
409 permeabilized in 10 μg/mL Proteinase-K/0.1% SDS/PBSTx, washed into x 0.1 M Triethanolamine
410 pH7-8 (TEA), 2.5 μL/mL acetic anhydride was added for 5 min with vigorous swirling, acetic
411 anhydride step was repeated, washed in PBSTx and post-fixed in 4% formaldehyde/PBSTx for 10
412 min. Probe synthesis, hybridization, and staining were performed as previously described[36] using
413 probe concentrations at ~50 ng/mL for 16-48 hrs at 56°C. All probes were synthesized with either
414 DIG or DNP haptens and detected using the following antibodies, all at 1:2000: anti-DIG-AP
415 (Sigma), anti-DIG-POD (Roche), anti-DNP-HRP (Vector Labs). Colorimetric development was
416 done using NBT (Roche)/BCIP (Sigma) or with Fast-Blue (Sigma)[38]. Fluorescent signal was
417 visualized after TSA reaction[36]. DAPI staining and mounting were performed as described above.

418

419 Microscopy

420 Confocal imaging was performed on a Zeiss LSM 880 with the following objectives: 10X
421 PlanNEOFLUOR air, NA 0.3/ 20X Plan-APOCHROMAT air, NA 0.8/ 40X C-APOCHROMAT
422 oil, NA 1.3/ 63X Plan-APOCHROMAT oil, NA 1.4. WISH samples and whole-mount DAPI-
423 stained worms were imaged using a Zeiss AxioZoom V16. Image processing was performed using
424 ImageJ.

425

426 RNAi

427 Double-stranded RNA (dsRNA) was synthesized as previously described[39] and
428 resuspended at concentrations ~ 1.5-2 μg/μL. For control injections, 1.5 kb dsRNA derived from
429 an irrelevant bacterial sequence was used. 6-day old tapeworms were obtained and microinjected
430 with dsRNA using femtotips II via the Femtojet injection system (Eppendorf) to obtain spreading
431 across the first ~ 3-4 mm anterior of the tapeworm. The spread of injected fluids could be detected
432 by a temporary increase in opacity. 500 hPa injection pressure for 0.3-0.8 ms was used per injection
433 site. Whole tapeworms were cultured *in vitro* for 3 days and then 2 mm anterior fragments were
434 amputated and cultured for another 3 days. On day 6, the fragments were re-injected with dsRNA
435 throughout the whole fragment and returned to *in vitro* culture for 9 days before they were
436 terminated for analysis.

437

438 Cell transplantations

439 For dissociated cell preparations, tapeworms were placed in a drop of calcium-magnesium
440 free HBSS (CMF HBSS, Gibco), minced into small pieces with a tungsten needle, incubated in

441 3X Trypsin-EDTA (59418C, Sigma) in CMF HBSS for 20 min at 37°C and dissociated using a
442 dounce homogenizer (Kontes). Cells were pelleted by centrifugation at 250 g for 5 min. The cell
443 pellet was washed in CMF HBSS and passed through cell strainers at 100 μm, 40 μm, 20 μm, and
444 10 μm (Falcon and Sysmex) with one spin and wash in between. Cells were pelleted and
445 resuspended in ~ 200-400 μL WH4 with 0.05% BSA. Cell injections were performed using the
446 Cell Tram Oil 4 injection system (Eppendorf) into the necks of irradiated worms. Injected worms
447 were cultured *in vitro* for 3 days before 5 mm anterior fragments were amputated and grown for
448 an additional 27 days.

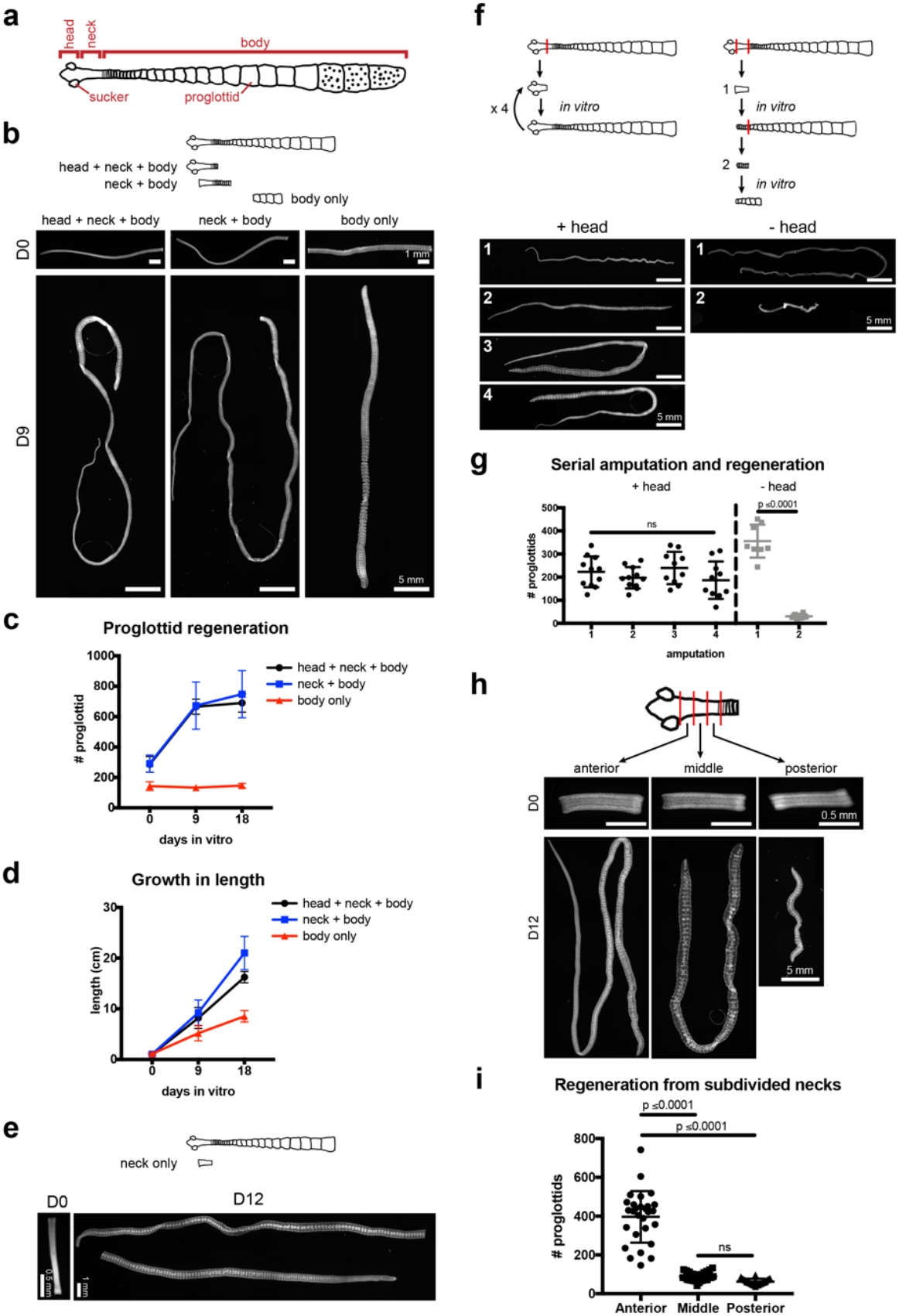
a
head
neck
body
sucker
proglottid
b
head + neck + body
neck + body
body only
head + neck + body
neck + body
body only
D0
D9
1 mm
5 mm
c
Proglottid regeneration
proglottid
days in vitro
head + neck + body
neck + body
body only
d
Growth in length
length (cm)
days in vitro
head + neck + body
neck + body
body only
e
neck only
D0
D12
0.5 mm
1 mm
f
x 4
in vitro
1
2
in vitro
+ head
- head
5 mm
g
Serial amputation and regeneration
+ head
- head
p ≤0.0001
ns
proglottids
amputation
h
anterior
middle
posterior
D0
D12
0.5 mm
5 mm
i
Regeneration from subdivided necks
p ≤0.0001
p ≤0.0001
ns
proglottids
Anterior
Middle
Posterior

449

450 **Figure 1. Regeneration competence of *H. diminuta*. a**, Schematic of *H. diminuta* adults. The
451 tapeworm head includes suckers that attach the worm to the intestine. The neck is defined as the
452 unsegmented region between the head and body. The proglottids grow in an anterior-to-posterior
453 direction and increase in reproductive maturity as they are displaced posteriorly. The most
454 posterior proglottids are gravid with embryos (dotted). We used 6-day old tapeworms that were
455 not yet gravid. **b**, DAPI-stained 1 cm tapeworm fragments before and after 9 days in culture. **c-d**,
456 Quantification of proglottid number and growth in length from (**b**). Error bars=SD, N=2-5, n=7-
457 21 for each timepoint and condition. **e**, Representative DAPI-stained "neck only" fragments before
458 and after 12 days *in vitro*. **f-g**, DAPI-stained fragments after serial amputation. 2 mm anterior
459 fragments, with or without the head, were grown *in vitro* for 12-15 days and then re-amputated
460 serially. Error bars=SD, one-way ANOVA for +head samples, t-test for -head samples. **h-i**, The
461 neck was subdivided into 1 mm fragments from the anterior, middle, and posterior of the neck and
462 grown *in vitro*. DAPI-stained worms are shown. Error bars=SD, N=3, n=22-29 per condition, one-
463 way ANOVA.

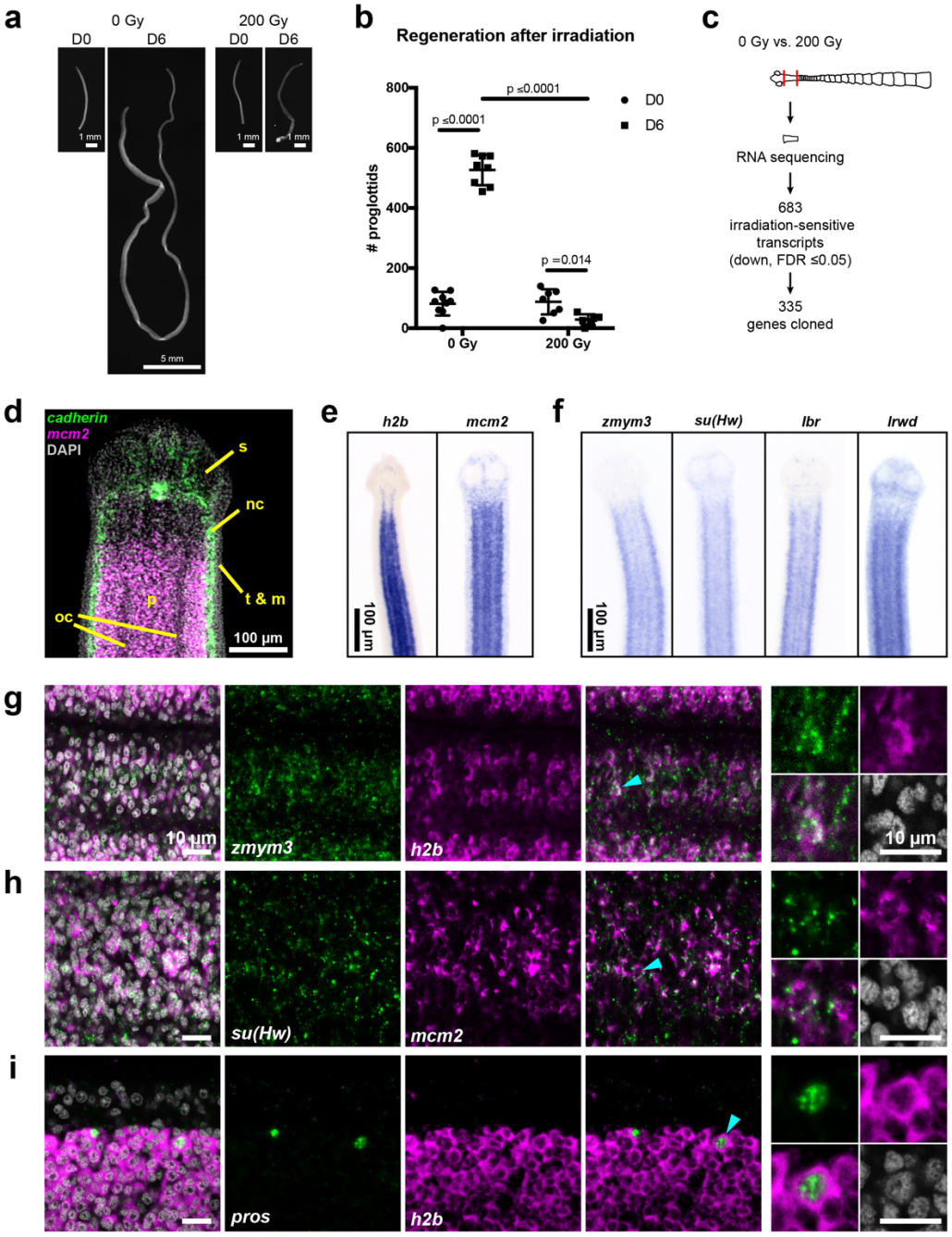

Figure 2. Identification of cycling somatic cell genes using RNA-seq. a-b, DAPI staining of 5 mm anterior fragments from control and irradiated worms before and after *in vitro* culture for 6 days. Error bars=SD, one-way ANOVA. **c**, Schematic of RNA-seq strategy to identify irradiation-sensitive transcripts. **d**, Confocal section of a tapeworm anterior. Cycling cells marked by *mcm2* (magenta) are confined to the neck parenchyma between the nerve cords marked by *cadherin* (green). (s: sucker, nc: nerve cord, oc: osmoregulatory canal, t: tegument, m: muscle, and p: parenchyma). **e**, WISH of known cycling cell markers *h2b* and *mcm2*. **f**, WISH for genes expressed in the neck parenchyma similar to *h2b* and *mcm2*. **g-i**, Confocal sections of dFISH for irradiation-sensitive genes (green) with *h2b* or *mcm2* (magenta). Cyan arrowheads indicate cells that are magnified at the far right.

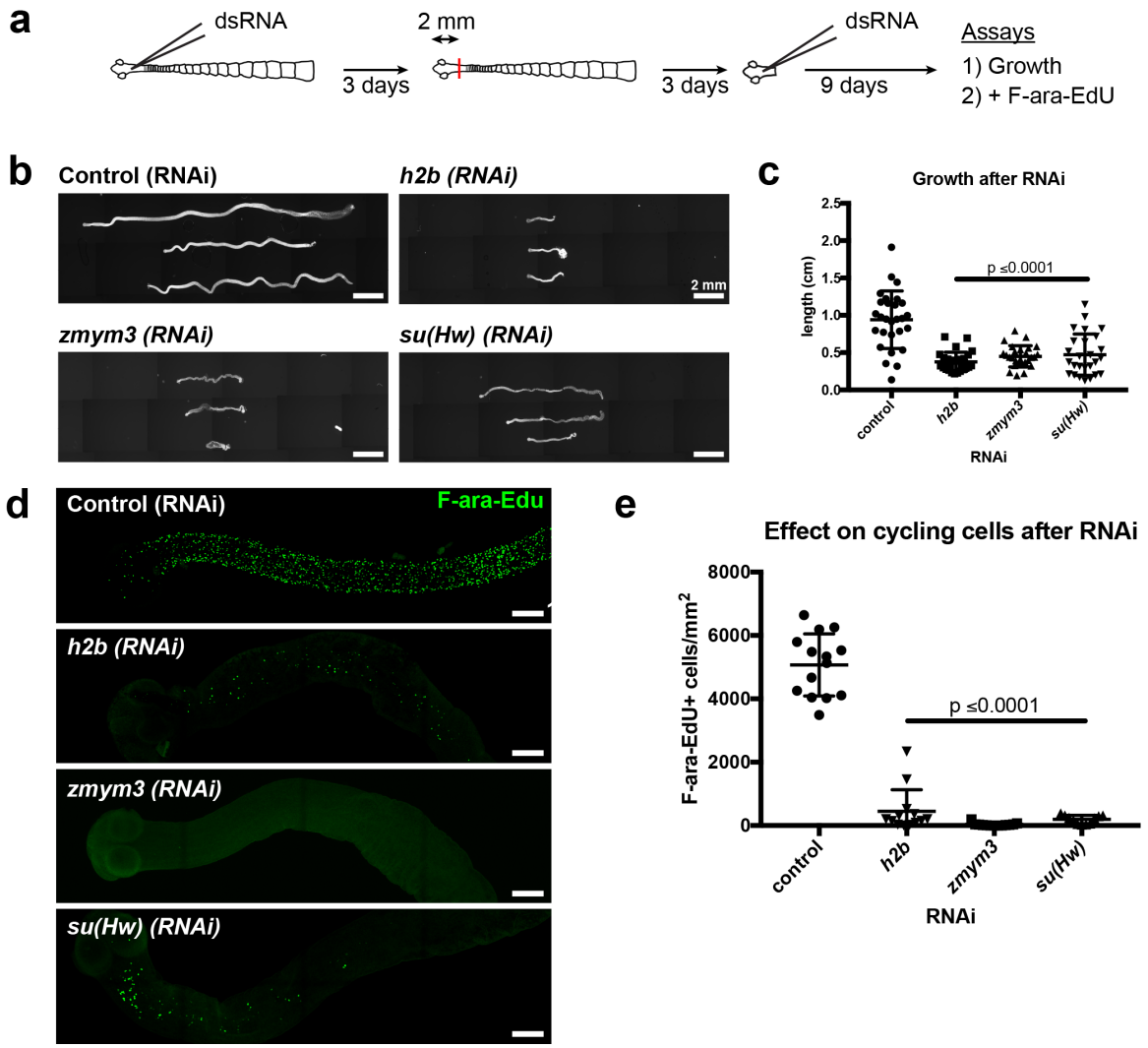

Figure 3. RNAi to identify genes required for proper growth and regeneration in *H. diminuta*. **a**, Schematic of RNAi paradigm. **b**, DAPI-stained worms after RNAi knockdown of *h2b, zmym3*, or *su(Hw)*. **c**, Quantification of worm lengths after RNAi. Error bars=SD, N=3-4, n=26-37, one-way ANOVA. **d**, Maximum-intensity projections from confocal z-stacks at tapeworm necks after RNAi. Panels are oriented anterior facing left. **e**, Quantification of (**d**). Number of F-ara-EdU^{+} cells was normalized to total area from maximum-intensity projection of the DAPI stain. Error bars=SD, N=3, n=11-14, one-way ANOVA.

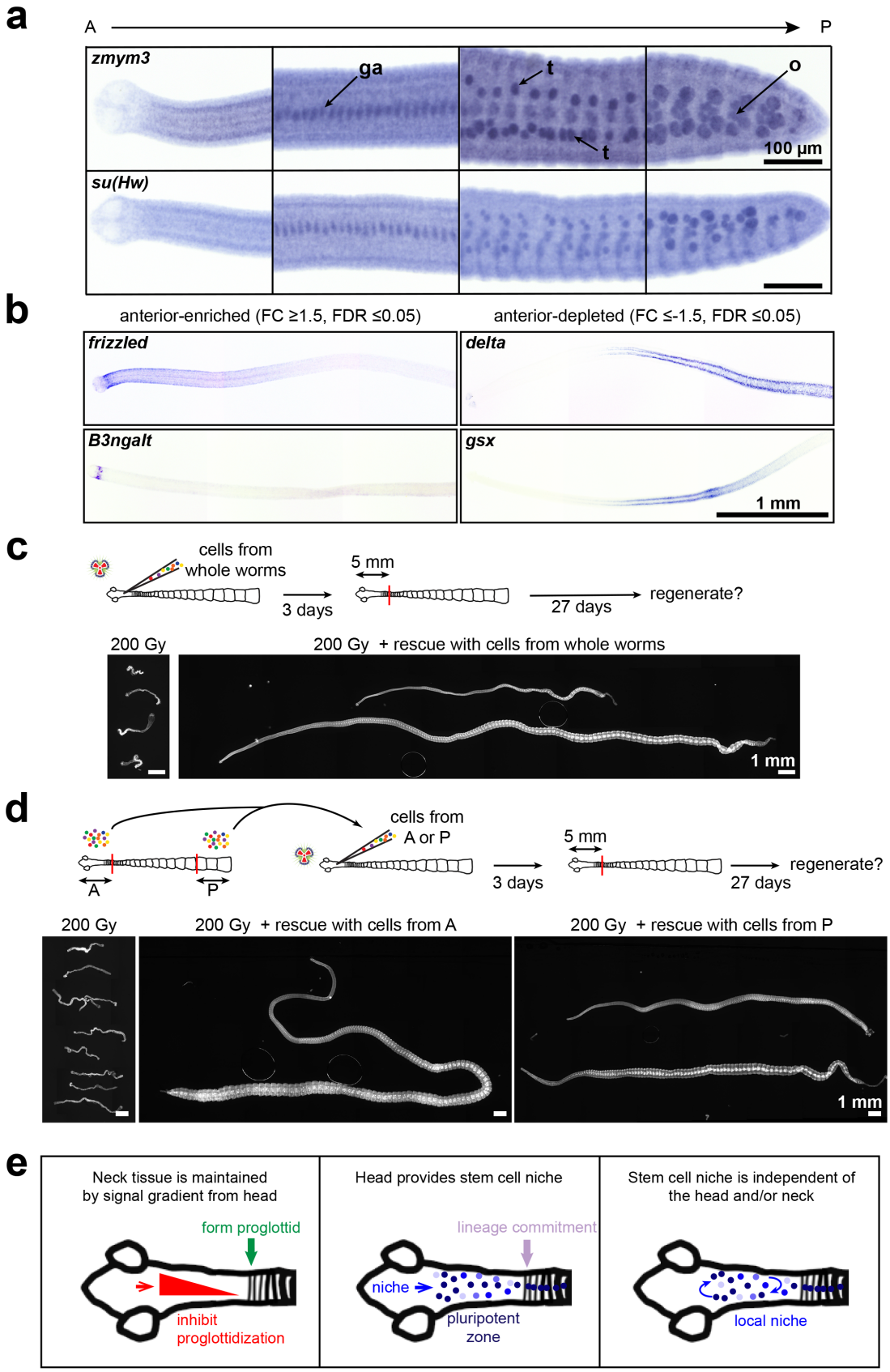
a
A
P
zmym3
ga
t
t
o
100 µm
su(Hw)
b
anterior-enriched (FC ≥1.5, FDR ≤0.05)
anterior-depleted (FC ≤-1.5, FDR ≤0.05)
frizzled
delta
B3ngalt
gsx
1 mm
c
cells from
whole worms
3 days
5 mm
27 days
regenerate?
200 Gy
200 Gy + rescue with cells from whole worms
1 mm
d
A
P
cells from
A or P
3 days
5 mm
27 days
regenerate?
200 Gy
200 Gy + rescue with cells from A
200 Gy + rescue with cells from P
1 mm
e
Neck tissue is maintained
by signal gradient from head
form proglottid
inhibit
proglottidization
Head provides stem cell niche
lineage commitment
niche
pluripotent
zone
Stem cell niche is independent of
the head and/or neck
local niche

483

484 **Figure 4. Rescue of lethally irradiated tapeworms by cell transplantation. a**, WISH patterns
485 for cycling cell genes across the tapeworm A-P axis (ga: genital anlagen; t: testis; o: ovary). **b,**
486 WISH at tapeworm anteriors for genes that were anteriorly enriched or anteriorly depleted by
487 RNA-seq across the A-P axis of the neck only (refer to Fig. 1h). Panels are oriented anterior facing
488 left. **c**, DAPI-stained worms after rescue with cell transplants from whole worms. **d**, DAPI-stained
489 worms after rescue with cell transplants sourced from 5 mm anteriors (A) or 5 mm posteriors (B).
490 **e**, Models for how region-specific regeneration is regulated in *H. diminuta.*

491 **Supplemental Figures**

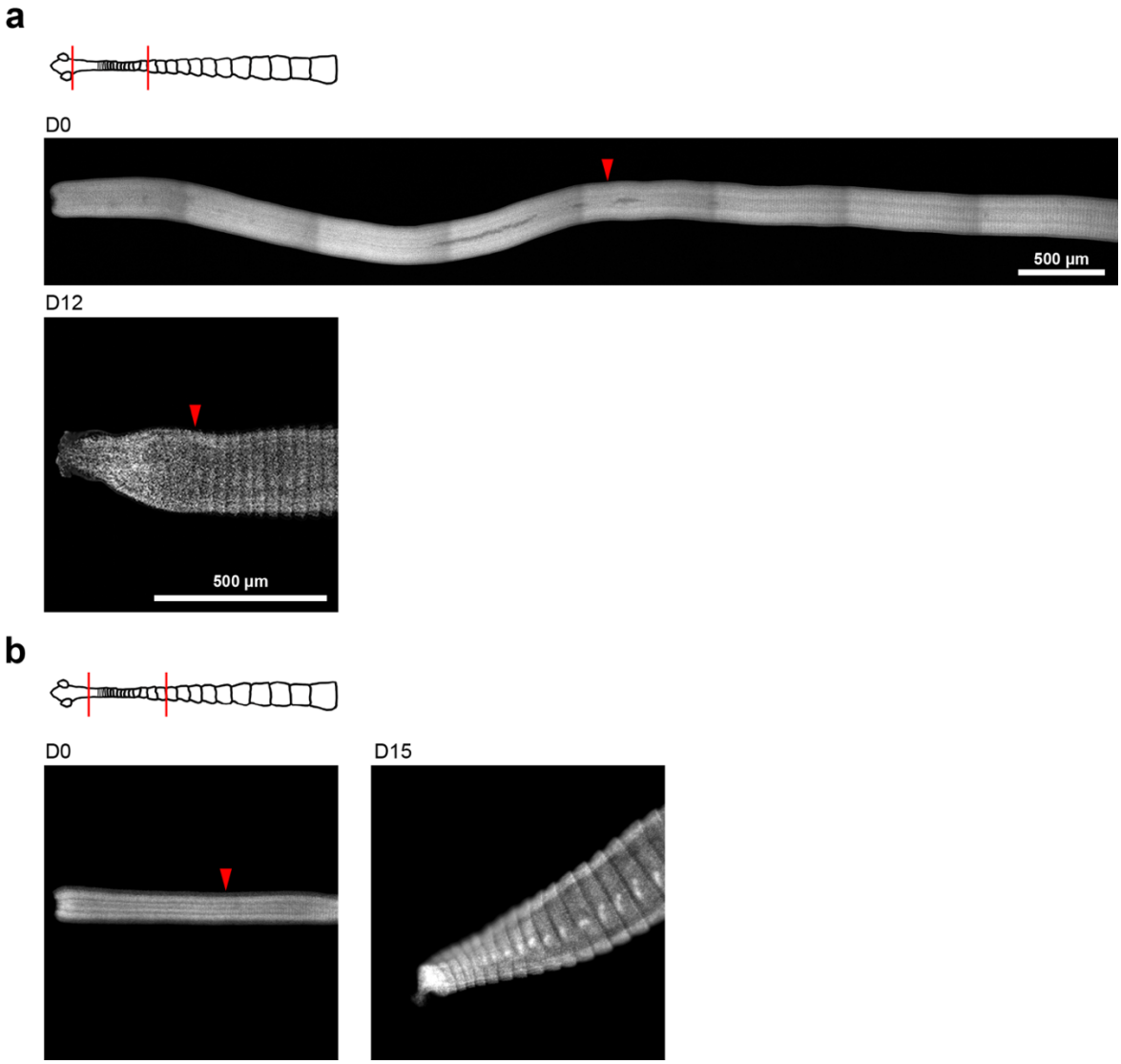

492

493 **Figure S1. Unsegmented neck is depleted after decapitation. a-b**, DAPI-stained worms after
494 decapitation cultured *in vitro* for the indicated number of days. Red arrowheads mark the position
495 of the first visible proglottid. **b**, Worms were amputated 2 mm posterior to the head to remove
496 most of the neck tissue before culturing. After 15 days *in vitro* the neck tissue is no longer
497 identifiable.

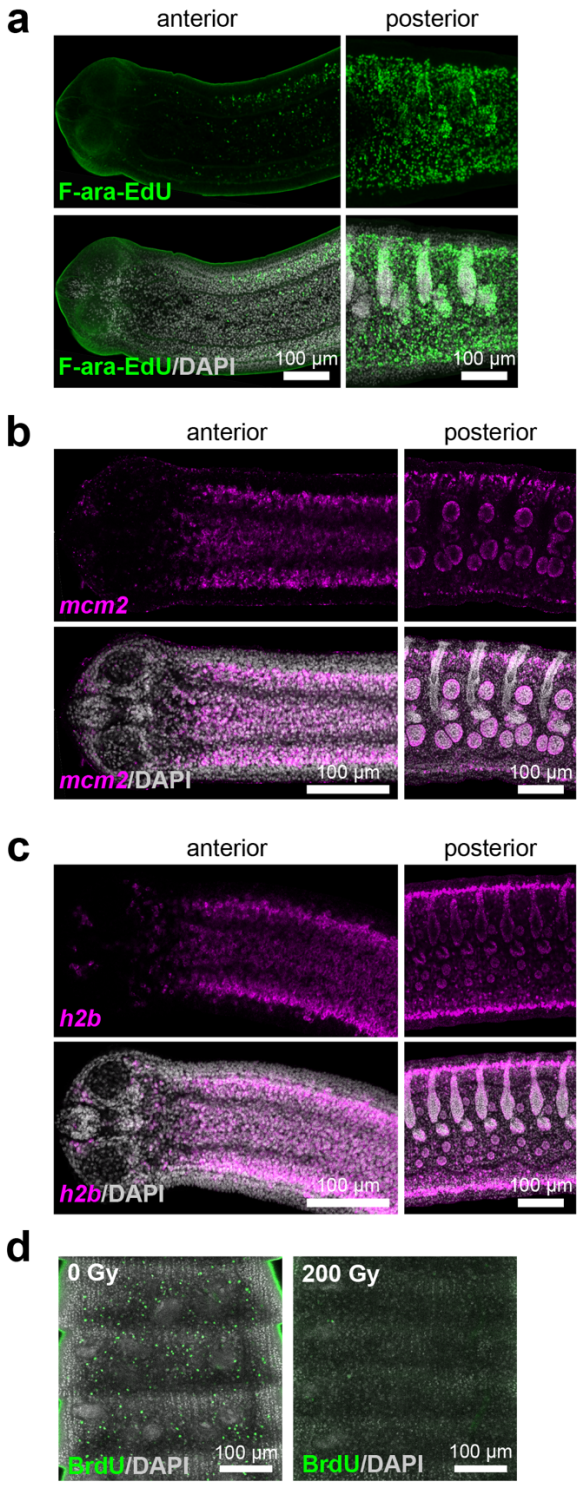

Figure S2. Cycling somatic cells are distributed throughout the whole tapeworm body and are irradiation sensitive. a-c, Confocal sections after uptake of F-ara-Edu for 1 hr (**a**) or FISH to detect *mcm2* (**b**) or *h2b* (**c**). Panels are oriented anterior facing left. **d,** Confocal sections of BrdU labeled tapeworms +/- irradiation. Uptake of BrdU for 1 hr, through a section in the worm body after exposure to 200 Gy irradiation.

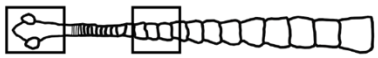

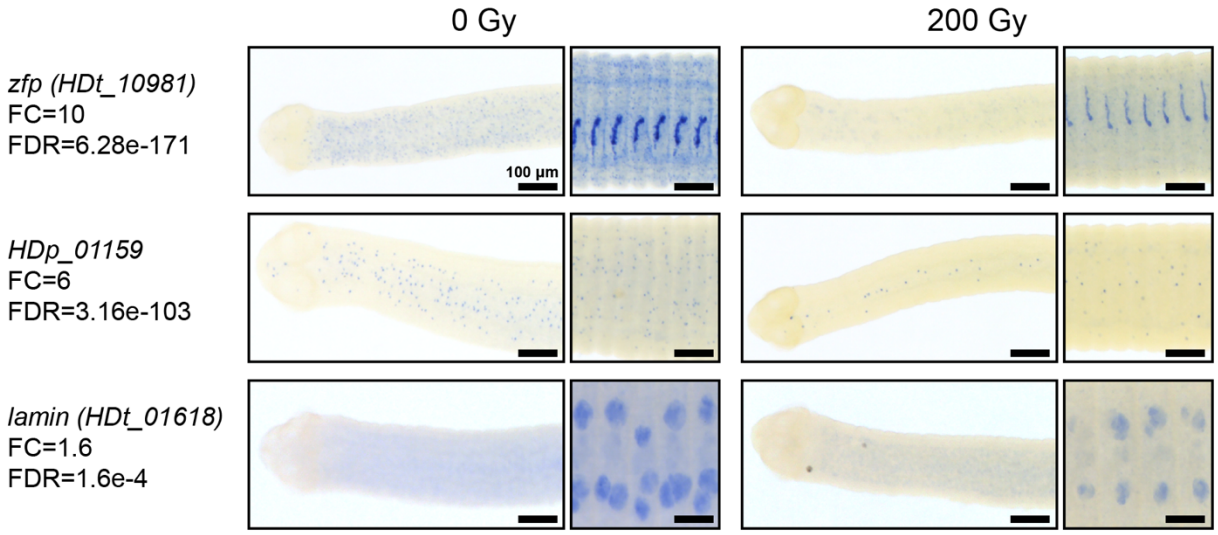

Figure S3. Validation of RNA-seq results by WISH after irradiation. WISH from two regions of the tapeworm: anterior (left) and body (right), +/- exposure to irradiation followed by 3 days *in vitro*.

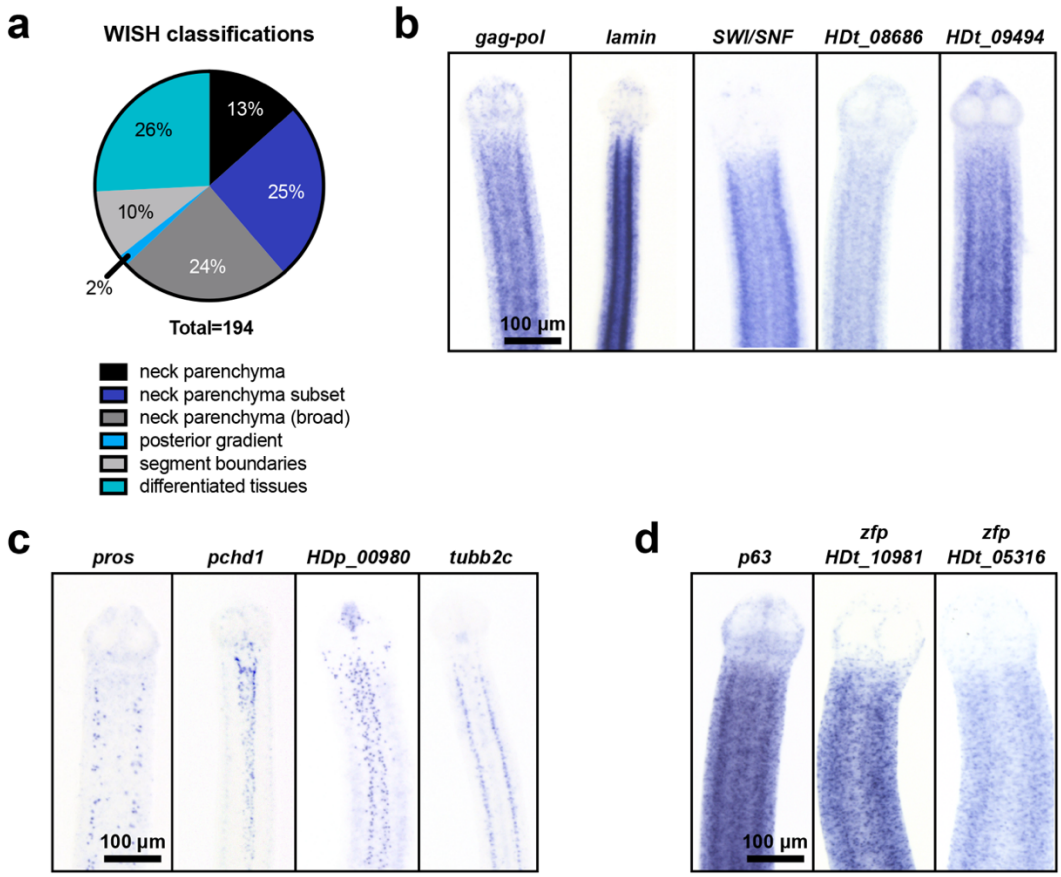

Figure S4. WISH patterns of potential cycling cell genes identified using RNA-seq. a, Classification of WISH expression patterns. **b-d**, WISH patterns at tapeworm necks with anterior oriented up. **b**, Examples of genes expressed in the neck parenchyma. **c**, Examples of genes expressed in a subset of cells within the neck. **d**, Examples of genes expressed broadly in the neck including toward the animal edge where differentiated muscle and tegument are located.

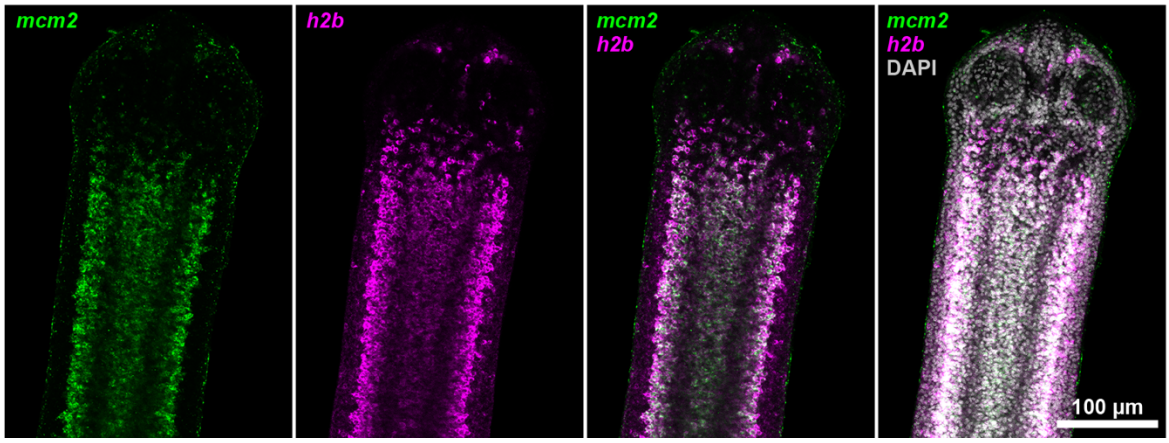

Figure S5. Colocalization of *mcm2* and *h2b*. Confocal section of dFISH to detect *mcm2* (green) and *h2b* (magenta) in the neck parenchyma. Panels are oriented anterior up.

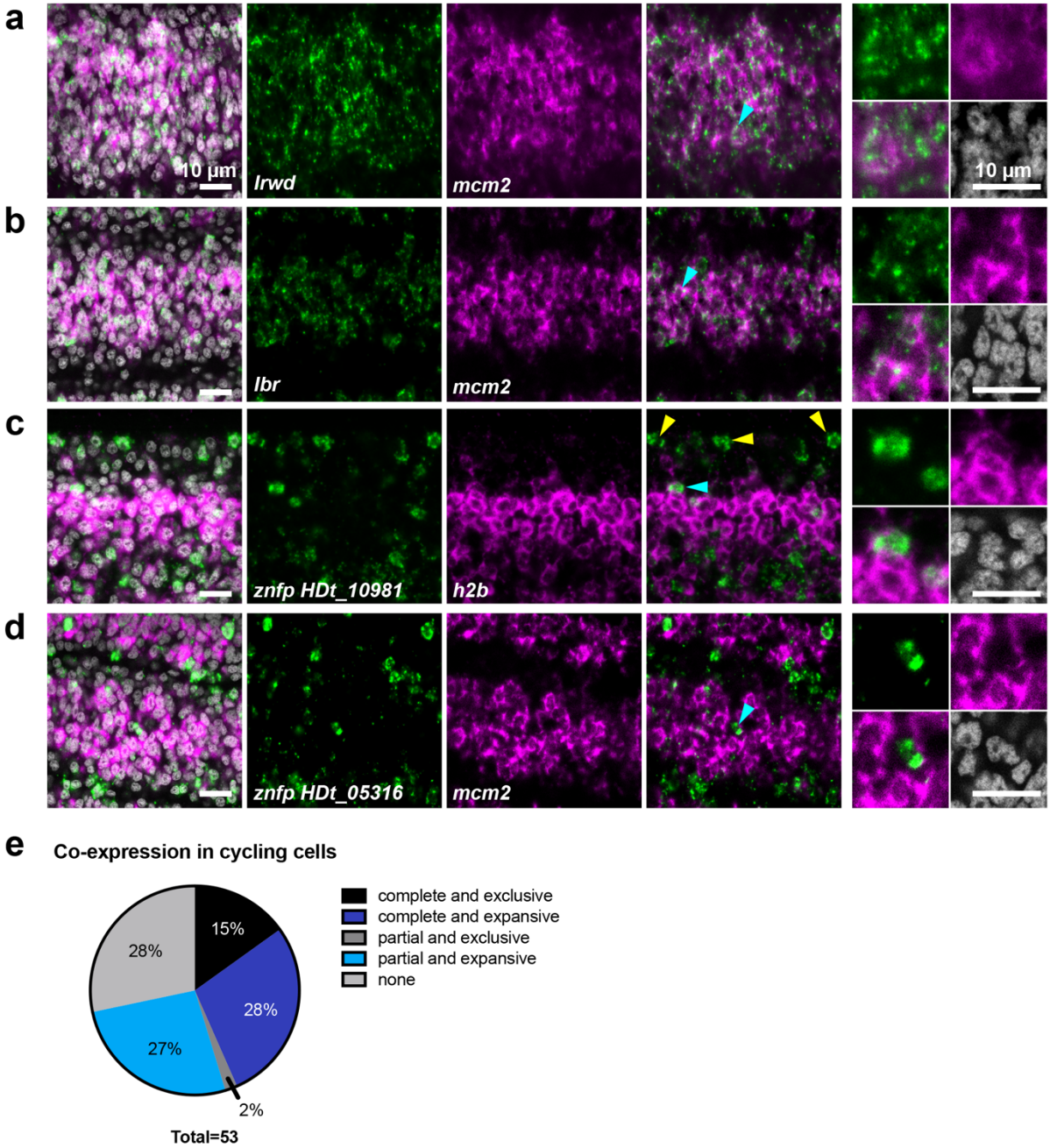

Figure S6. The cycling somatic cell population is heterogeneous. a-d, Confocal sections of dFISH to detect irradiation-sensitive genes (green) with *h2b* or *mcm2* (magenta). Cyan arrowheads indicate cells that are magnified at the far right. Yellow arrowheads point to examples of expression in non-cycling cells. **e**, Summary of different co-expression patterns obtained from 53 dFISH experiments.

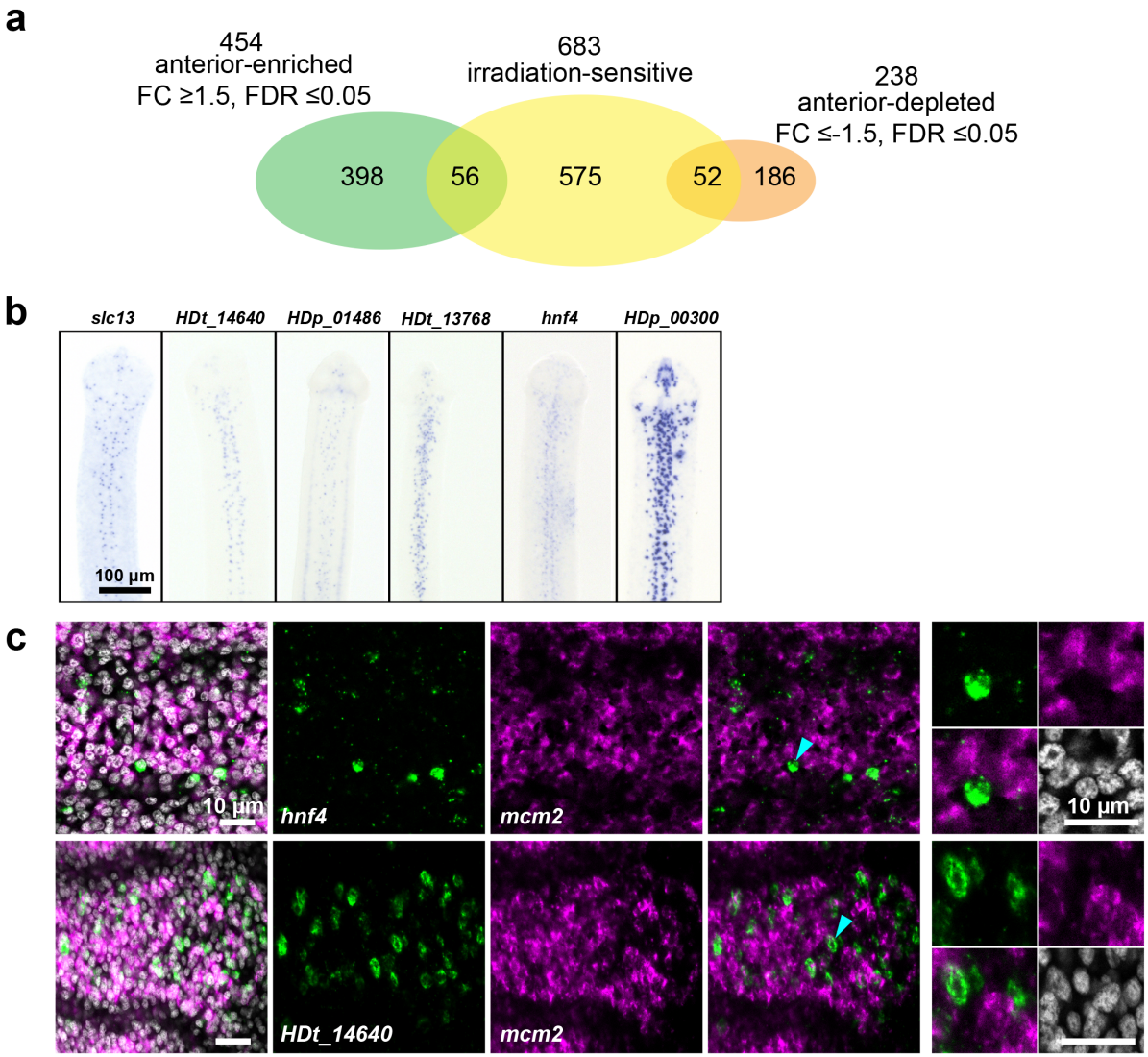

Figure S7. RNA-seq identifies anterior-enriched genes that are expressed predominantly in non-cycling cells. a, Differential gene expression analysis of anterior, middle, and posterior neck fragments from Fig. 1h was used to identify anterior-enriched and anterior-depleted transcripts. Transcripts were considered anteriorly enriched if they were upregulated in the anterior vs. middle or posterior fragments with fold change ≥1.5 and FDR ≤0.05 and conversely for anterior-depleted transcripts. Overlap with irradiation-sensitive transcripts is shown. **b**, WISH of genes that were anteriorly enriched and irradiation sensitive. All panels are oriented with anterior facing up. **c**, Confocal sections of dFISH to detect genes from (**b**), with *mcm2* (magenta). Cyan arrowheads indicate cells that are magnified at the far right.

534 **References**

535 1. Roberts, L. S. The influence of population density on patterns and physiology of growth in
536 *Hymenolepis diminuta* (Cestoda:Cyclophyllidea) in the definitive host. *Exp. Parasitol.* **11,**
537 332–371 (1961).
538 2. Del Brutto, O. H. Human cysticercosis (*Taenia solium*). *Trop Parasitol* **3,** 100–103
539 (2013).
540 3. Craig, P. & Ito, A. Intestinal cestodes. *Curr. Opin. Infect. Dis.* **20,** 524–532 (2007).
541 4. Arai, H. P. *Biology of the Tapeworm Hymenolepis diminuta*. (Academic Press, Inc., 1980).
542 5. Read, C. P. Longevity of the tapeworm, *Hymenolepis diminuta*. *J. Parasitol.* **53,** 1055–
543 1056 (1967).
544 6. Newmark, P. A. & Sánchez Alvarado, A. Not Your Father's Planarian: A Classic Model
545 Enters The Era Of Functional Genomics. *Nat. Rev. Genet.* **3,** 210–219 (2002).
546 7. Reddien, P. W. The Cellular and Molecular Basis for Planarian Regeneration. *Cell* **175,**
547 327–345 (2018).
548 8. Baguñà, J. The planarian neoblast: the rambling history of its origin and some current
549 black boxes. *Int. J. Dev. Biol.* **56,** 19–37 (2012).
550 9. Roberts, L. S. Development of *Hymenolepis diminuta* in its definitive host in *Biology of*
551 *the Tapeworm Hymenolepis Diminuta,* 357–423 (Academic Press, Inc., 1980).
552 10. Collins, J., III *et al.* Adult somatic stem cells in the human parasite *Schistosoma mansoni*.
553 *Nature* **494,** 476–479 (2013).
554 11. Koziol, U., Rauschendorfer, T., Zanon Rodríguez, L., Krohne, G. & Brehm, K. The
555 unique stem cell system of the immortal larva of the human parasite *Echinococcus*
556 *multilocularis*. *EvoDevo* **5,** 10 (2014).
557 12. Wang, B., Collins, J., III & Newmark, P. A. Functional genomic characterization of
558 neoblast-like stem cells in larval *Schistosoma mansoni*. *eLife* **2,** e00768 (2013).
559 13. Tsai, I. J. *et al.* The genomes of four tapeworm species reveal adaptations to parasitism.
560 *Nature* **496,** 57–63 (2013).
561 14. Brehm, K. & Koziol, U. On the importance of targeting parasite stem cells in anti-
562 echinococcosis drug development. *Parasite* **21,** 72 (2014).
563 15. Goodchild, C. G. Transfaunation and repair of damage in the rat tapeworm, *Hymenolepis*
564 *diminuta*. *J. Parasitol.* **44,** 345–351 (1958).
565 16. Schiller, E. L. A simplified method for the in vitro cultivation of the rat tapeworm,
566 *Hymenolepis diminuta*. *J. Parasitol.* **51,** 516–518 (1965).
567 17. Bolla, R. I. & Roberts, L. S. Developmental physiology of cestodes. IX. Cytological
568 characteristics of the germinative region of *Hymenolepis diminuta*. *J. Parasitol.* **57,** 267–
569 277 (1971).
570 18. Sulgostowska, T. The development of organ systems in cestodes. I. A study of histology
571 of *Hymenolepis diminuta* (Rudolphi, 1819) (Hymenolepididae). *Acta Parasitologica*
572 *Polonica* **20,** 449–462 (1972).
573 19. Solana, J. *et al.* Defining the molecular profile of planarian pluripotent stem cells using a
574 combinatorial RNAseq, RNA interference and irradiation approach. *Genome Biol.* **13,** R19
575 (2012).
576 20. Eisenhoffer, G. T., Kang, H. & Sánchez Alvarado, A. Molecular analysis of stem cells and
577 their descendants during cell turnover and regeneration in the planarian *Schmidtea*
578 *mediterranea*. *Cell Stem Cell* **3,** 327–339 (2008).

579 21. Koziol, U. & Castillo, E. Cell proliferation and differentiation in cestodes. *Research in*
580 *Helminths* 121–138 (2011).
581 22. Collins, J., III, Wendt, G. R., Iyer, H. & Newmark, P. A. Stem cell progeny contribute to
582 the schistosome host-parasite interface. *eLife* **5,** 243 (2016).
583 23. Pierson, L. *et al.* RNA interference in a cestode reveals specific silencing of selected
584 highly expressed gene transcripts. *Int. J. Parasitol.* **40,** 605–615 (2010).
585 24. Mizukami, C. *et al.* Gene silencing in *Echinococcus multilocularis* protoscoleces using
586 RNA interference. *Parasitol. Int.* **59,** 647–652 (2010).
587 25. Spiliotis, M. *et al. Echinococcus multilocularis* primary cells: improved isolation, small-
588 scale cultivation and RNA interference. *Mol. Biochem. Parasitol.* **174,** 83–87 (2010).
589 26. Pouchkina-Stantcheva, N. N., Cunningham, L. J., Hrčkova, G. & Olson, P. D. RNA-
590 mediated gene suppression and in vitro culture in *Hymenolepis microstoma*. *Int. J.*
591 *Parasitol.* **43,** 641–646 (2013).
592 27. Hu, X. *et al.* Gene knockout of *Zmym3* in mice arrests spermatogenesis at meiotic
593 metaphase with defects in spindle assembly checkpoint. *Cell Death Dis* **8,** e2910 (2017).
594 28. Leung, J. W. C. *et al.* ZMYM3 regulates BRCA1 localization at damaged chromatin to
595 promote DNA repair. *Genes Dev.* **31,** 260–274 (2017).
596 29. Gdula, D. A., Gerasimova, T. I. & Corces, V. G. Genetic and molecular analysis of the
597 gypsy chromatin insulator of *Drosophila*. *Proc. Natl. Acad. Sci. U.S.A.* **93,** 9378–9383
598 (1996).
599 30. Sikes, J. M. & Newmark, P. A. Restoration of anterior regeneration in a planarian with
600 limited regenerative ability. *Nature* **500,** 77–80 (2013).
601 31. Liu, S. Y. *et al.* Reactivating head regrowth in a regeneration-deficient planarian species.
602 *Nature* **500,** 81–84 (2013).
603 32. Umesono, Y. *et al.* The molecular logic for planarian regeneration along the anterior-
604 posterior axis. *Nature* **500,** 73–76 (2013).
605 33. Koziol, U., Jarero, F., Olson, P. D. & Brehm, K. Comparative analysis of Wnt expression
606 identifies a highly conserved developmental transition in flatworms. *BMC Biol.* **14,** 1
607 (2016).
608 34. Forsthoefel, D. J. *et al.* An RNAi screen reveals intestinal regulators of branching
609 morphogenesis, differentiation, and stem cell proliferation in planarians. *Dev. Cell* **23,**
610 691–704 (2012).
611 35. Collins, J., III, King, R. S., Cogswell, A., Williams, D. L. & Newmark, P. A. An atlas for
612 *Schistosoma mansoni* organs and life-cycle stages using cell type-specific markers and
613 confocal microscopy. *PLoS Negl Trop Dis* **5,** e1009 (2011).
614 36. King, R. S. & Newmark, P. A. In situ hybridization protocol for enhanced detection of
615 gene expression in the planarian *Schmidtea mediterranea*. *BMC Dev. Biol.* **13,** 8 (2013).
616 37. Salic, A. & Mitchison, T. J. A chemical method for fast and sensitive detection of DNA
617 synthesis in vivo. *Proceedings of the National Academy of Sciences* **105,** 2415–2420
618 (2008).
619 38. Currie, K. W. *et al.* HOX gene complement and expression in the planarian *Schmidtea*
620 *mediterranea*. *EvoDevo* **7,** 7 (2016).
621 39. Rouhana, L. *et al.* RNA interference by feeding in vitro-synthesized double-stranded RNA
622 to planarians: methodology and dynamics. *Dev. Dyn.* **242,** 718–730 (2013).